Letter

Manipulating synthetic gauge fluxes via multicolor dressing of Rydberg-atom arrays

Xiaoling Wu,[1,*] Fan Yang,[2,*,†] Shuo Yang,[1,3,4,5,‡] Klaus Mølmer,[2,6] Thomas Pohl,[2]
Meng Khoon Tey,[1,3,4,5] and Li You[1,3,4,5,7,§]

[1]*Department of Physics, State Key Laboratory of Low Dimensional Quantum Physics, Tsinghua University, Beijing 100084, China*
[2]*Department of Physics and Astronomy, Center for Complex Quantum Systems, Aarhus University, DK-8000 Aarhus C, Denmark*
[3]*Frontier Science Center for Quantum Information, Beijing 100084, China*
[4]*Collaborative Innovation Center of Quantum Matter, Beijing 100084, China*
[5]*Hefei National Laboratory, Hefei 230088, China*
[6]*Aarhus Institute of Advanced Studies, Aarhus University, DK-8000 Aarhus C, Denmark*
[7]*Beijing Academy of Quantum Information Sciences, Beijing 100193, China*

(Received 4 March 2022; accepted 7 September 2022; published 28 September 2022)

Arrays of highly excited Rydberg atoms can be used as powerful quantum simulation platforms. Here, we introduce an approach that makes it possible to implement fully controllable effective spin interactions in such systems. We show that optical Rydberg dressing with multicolor laser fields opens up distinct interaction channels that enable complete site-selective control of the induced interactions and favorable scaling with respect to decoherence. We apply this method to generate synthetic gauge fields for Rydberg excitations where the effective magnetic flux can be manipulated at the single-plaquette level by simply varying the phase of the local dressing field. The system can be mapped to a highly anisotropic Heisenberg model, and the resulting spin interaction opens the door for explorations of topological phenomena with nonlocal density interactions. A remarkable consequence of the interaction is the emergence of topologically protected long-range doublons, which exhibit strongly correlated motion in a chiral and robust manner.

DOI: 10.1103/PhysRevResearch.4.L032046

Quantum simulators make it possible to solve many-body problems that are otherwise intractable by classical calculations [1]. An important class of such problems arises from quantum lattice models in external gauge fields in which a host of exotic phases have been predicted, ranging from fractional quantum Hall effects [2–4] to chiral spin liquids [5–8]. The technological and fundamental significance of such topological phases of matter has motivated significant efforts towards implementing strong synthetic gauge fields in different physical systems [9–26].

Rydberg atoms, held in optical lattices or arrays of optical tweezers, are currently among the most promising and versatile simulation platforms for quantum magnetism [27–34]. Realizing an effective magnetic flux for Rydberg excitations requires a complex-valued exchange interaction between different atomic states. This can be accomplished via a proper tuning of dipolar exchange interactions between different Rydberg states [35]. By applying a real magnetic field, the intrinsic spin-orbit coupling of such interactions [36] can be used to generate an effective spin-lattice model with a nonvanishing Peierls phase that emerges perturbatively to leading order in the strength of the dipole-dipole interaction. The possibility to engineer synthetic gauge fields in interacting spin lattices then holds exciting perspectives for exploring exotic many-body phases and dynamics [37–41].

Here, we describe an approach to implementing synthetic gauge fields via photon-assisted excitation exchange in Rydberg-atom arrays. Dressing the atoms by multicolor laser fields is shown to offer complete optical control of the generated spin-exchange interactions at the level of individual sites. The induced Peierls phase is determined by the relative phase between the applied laser fields with which the effective gauge flux can be tuned to arbitrary patterns. Together with the nonlocal density interaction between Rydberg excitations, this yields a versatile quantum simulation approach for exploring strongly correlated systems with nontrivial band topologies and finite-range interactions. We illustrate these perspectives by discussing the topologically protected chiral motion of bound pairs [42–44] that emerge from the multicolor Rydberg dressing of an atomic square lattice [45].

We consider a two-dimensional array of individually trapped atoms. For a monochromatic Rydberg dressing [46], the ground-state $|g_i\rangle$ of the ith atom (located at $\mathbf{r}_i$) is coupled to a Rydberg state $|r_i\rangle$ by an off-resonant laser field with Rabi frequency $\Omega_i = |\Omega_i|e^{i\varphi_i}$ and detuning $\Delta = \omega_0 - \omega_L$, where ω_0 and ω_L are the atomic transition frequency and laser frequency, respectively. Let us first consider a two-atom model [see Fig. 1(a)]. In this case, the singly excited pair states $|g_i r_j\rangle$ and $|r_i g_j\rangle$ are degenerate and coupled by two Raman pathways

*These authors contributed equally to this work.
†fanyang@phys.au.dk
‡shuoyang@mail.tsinghua.edu.cn
§lyou@mail.tsinghua.edu.cn

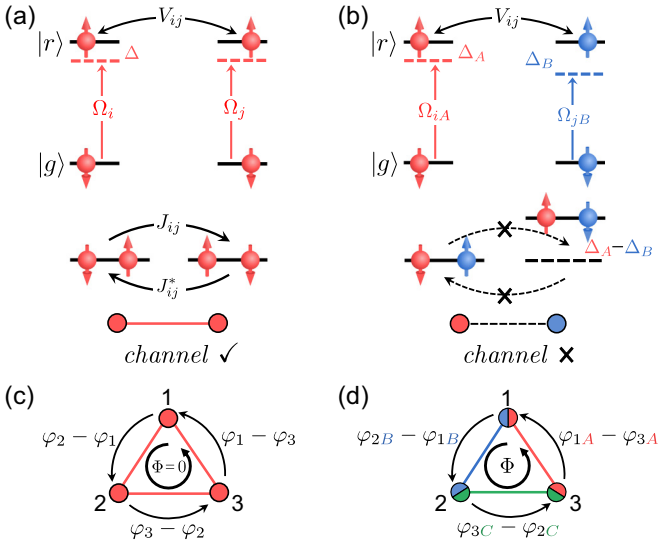

FIG. 1. (a) An excitation hopping channel between atoms can be established with monochromatic Rydberg dressing. (b) Lasers with different colors (frequencies) A and B cannot form a hopping channel due to the large energy defect $|\delta E| = |\Delta_A - \Delta_B|$. (c) Cancellation of the Peierls phase leads to a vanishing magnetic flux $\Phi = 0$ in monochromatic dressing. (d) A tunable flux Φ is realized by the multicolor dressing. Two-colored circles represent simultaneous dressing of the atoms by both laser fields of the colors indicated.

with intermediate states $|g_i g_j\rangle$ and $|r_i r_j\rangle$ [47,48]. Importantly, the contribution from both pathways is not symmetric because the doubly excited state $|r_i r_j\rangle$ is shifted by the van der Waals (vdW) interaction V_{ij} between Rydberg atoms. In the limit of large detunings, $|\Omega_{i(j)}| \ll |\Delta|, |\Delta + V_{ij}|$, this asymmetry leads to an effective hopping of the Rydberg excitation from site j to site i with a strength $|J_{ij}| = |\Omega_i \Omega_j^* V_{ij}/4\Delta(\Delta + V_{ij})|$. Taking into account the phase of each dressing field, this hopping amplitude $J_{ij} = |J_{ij}|e^{i\phi_{ij}}$ becomes complex with a Peierls phase $\phi_{ij} = \varphi_i - \varphi_j$ given by the sum of the phases φ_i and $-\varphi_j$ of both involved laser fields. However, it is impossible to induce a nonvanishing effective magnetic flux Φ because the same driving field creates and annihilates an excitation on each site, leading to a vanishing net flux as the excitation circulates around a closed loop. This is illustrated in Fig. 1(c) for three atoms whose total flux $\Phi = (\varphi_2 - \varphi_1) + (\varphi_3 - \varphi_2) + (\varphi_1 - \varphi_3) = 0$ vanishes identically.

As we will show below, a finite magnetic flux can, however, be realized by applying multiple dressing fields with different frequencies (colors). The underlying mechanism exploits the frequency sensitivity of the stimulated excitation exchange, which is only resonant if the two involved atoms share a set of dressing fields with identical colors. As illustrated in Fig. 1(d) for a three-atom plaquette, this makes it possible to independently control the phase of the exchange interaction between each atom pair with only three different colors A, B, C of the dressing fields applied, i.e., driving each atom with two different colors opens up a distinct interaction *channel* for each atom pair. The phase of each laser field can be tuned individually, such that we obtain a finite and tunable flux $\Phi = (\varphi_{2B} - \varphi_{1B}) + (\varphi_{3C} - \varphi_{2C}) + (\varphi_{1A} - \varphi_{3A})$. Here, we have

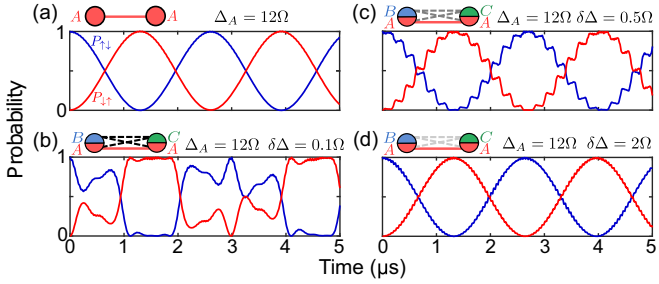

FIG. 2. Time evolution of excitation transport for monochromatic dressing in (a) and for multicolor dressing in (b)–(d) with increasing frequency separations $\delta\Delta = \Delta_B - \Delta_A = \Delta_C - \Delta_B$ between colors at induced hopping strength $|J| \approx 0.2\Omega$.

labeled the dressing fields of different colors by $\Theta \in \{A, B, \cdots\}$ and denote their phases at a given site i by $\varphi_{i\Theta}$.

We can gain more intuition by considering two atoms that are each dressed by fields with distinct detunings Δ_A and Δ_B [see Fig. 1(b)]. This implies a finite energy defect $\delta E = \Delta_A - \Delta_B$ for the excitation transfer between the states $|g_i r_j\rangle$ and $|r_i g_j\rangle$. The stimulated emission and reabsorption of photons is, thus, off-resonant by $|\delta E|$ and will suppress the excitation hopping if $|\delta E| \gg |J_{ij}|$. Under this condition we can introduce distinct interaction channels that only emerge when a pair of atoms is dressed by laser field with the same color $\Theta^{[ij]}$ [49], e.g., $\Theta^{[23]} = \{B, C\} \cap \{C, A\} = C$ for the configuration considered in Fig. 1(d). To verify that the cross talk between different colors can indeed be suppressed, we calculate the dynamics governed by the exact Hamiltonian,

$$\hat{H}_{\text{full}}(t) = \sum_i \hat{H}_i(t) + \sum_{i<j} V_{ij} |r_i\rangle\langle r_i| \otimes |r_j\rangle\langle r_j| \qquad (1)$$

for two dressed atoms. Here,

$$\hat{H}_i(t) = \sum_\Theta \left(\frac{\Omega_{i\Theta}}{2} e^{i\Delta_\Theta t} |r_i\rangle\langle g_i| + \text{H.c.} \right) \qquad (2)$$

describes the time-dependent single-particle Hamiltonian of the ith atom, and $V_{ij} = C_6/|\mathbf{r}_i - \mathbf{r}_j|^6$ denotes the vdW interaction between Rydberg excitations. As shown in Fig. 2(a), the excitation transport is nearly perfect for monochromatic dressing. The inclusion of two additional fields with different colors B and C, does not perturb this transport as long as the corresponding energy offset $|\Delta_\Theta - \Delta_{\Theta'}|$ is much larger than the respective hopping strength [Figs. 2(b)–2(d)]. With feasible experimental parameters [50], this condition can be well fulfilled, realizing a flux of $\Phi = \pi/2$ for the three-atom case considered in Fig. 1(d). This is verified by Fig. 3(a) where we find a characteristic chiral motion of the Rydberg excitation around the plaquette based on exact simulation of the dynamics. The simulation is in good agreement with an effective model that neglects any cross talk between different colors.

We can formulate the corresponding effective Hamiltonian by a perturbative analysis using Floquet theory [17,51–58]. Introducing bosonic creation operators $\hat{b}_i^\dagger = |r_i\rangle\langle g_i|$ with the hard-core constraint $\hat{b}_i^\dagger \hat{b}_i^\dagger = 0$, we obtain a single-excitation

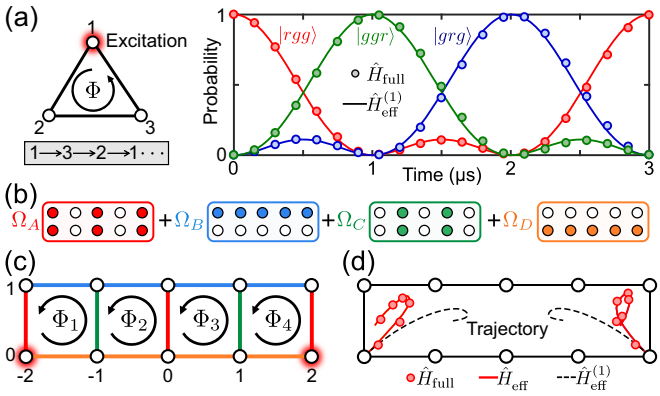

FIG. 3. (a) Single-excitation chiral motion in a three-atom plaquette at $\Phi = \pi/2$ with the chirality indicated by the gray box. (b) Dressing schemes to implement a Harper-Hofstadter lattice with an arbitrary flux pattern shown in (c). (d) Center-of-mass trajectories for an excitation in the left ($x \leqslant 0$) and right ($x \geqslant 0$) regions at $\Phi_1 = \Phi_4 = \pi/3$, $\Phi_2 = \Phi_3 = \pi/2$. The detunings are $(\Delta_A, \Delta_B, \Delta_C, \Delta_D) = 2\pi(120, 140, 160, 180)$ MHz in (a) and (d) with Rabi frequencies $(\Omega_A, \Omega_B, \Omega_C) = 2\pi(10, 10.9, 11.7)$ MHz in (a) and $(\Omega_A, \Omega_B, \Omega_C, \Omega_D) = 2\pi(10, 11.5, 13.1, 14.6)$ MHz in (d) [50].

effective Hamiltonian,

$$\hat{H}^{(1)}_{\text{eff}} = \sum_i \mu_i \hat{b}^\dagger_i \hat{b}_i + \sum_{i<j,\Theta^{[ij]}} (e^{i\phi_{ij\Theta^{[ij]}}} |J_{ij\Theta^{[ij]}}| \hat{b}^\dagger_i \hat{b}_j + \text{H.c.}), \tag{3}$$

where $\phi_{ij\Theta^{[ij]}} = \varphi_{i\Theta^{[ij]}} - \varphi_{j\Theta^{[ij]}}$ denotes the Peierls phase,

$$|J_{ij\Theta^{[ij]}}| = \left| \frac{\Omega_{i\Theta^{[ij]}} \Omega^*_{j\Theta^{[ij]}} V_{ij}}{4\Delta_{\Theta^{[ij]}}(\Delta_{\Theta^{[ij]}} + V_{ij})} \right| \tag{4}$$

is the hopping strength of the excitation, and μ_i is the on-site chemical potential. All these parameters can be tuned individually by adjusting the dressing fields at each site [49]. Importantly, the effective magnetic flux can be tuned by controlling the phase distribution of the applied dressing fields and does not depend on the laser intensities, lattice configurations, or Rydberg interactions. This makes it possible to generate an arbitrary magnetic flux pattern while implementing the effective Hamiltonian to an arbitrary accuracy by independently suppressing state leakages and crosstalk errors. Furthermore, the U(1) symmetry of the effective Hamiltonian Eq. (3) protects the system against various decoherence processes, e.g., global laser phase noise induced dephasing is eliminated in the resulting decoherence-free subspace [49,59,60], and the damping caused by decay of the Rydberg states can be mitigated by postselection as described in the Supplemental Material [49]. In the Supplemental Material [49], we show that the challenging single-site control of the laser intensity and phase distribution can be achieved by a compact optical module, whose complexity does not grow with system size. We also provide explicit schemes for manipulating gauge fluxes in different lattice geometries, including a square lattice, a triangular lattice, and a honeycomb lattice [49]. Altogether, this offers an accurate and scalable approach to synthesizing gauge fields with promising coherence properties.

Let us now discuss the behavior of multiple excitations, which feature strong vdW interactions between them. If the initial distance between excitations is sufficiently large such that their interactions V_{ij} are smaller than the detunings [49], the simple Hamiltonian,

$$\hat{H}_{\text{eff}} = \hat{H}^{(1)}_{\text{eff}} + \sum_{i<j} V_{ij} \hat{b}^\dagger_i \hat{b}^\dagger_j \hat{b}_j \hat{b}_i \tag{5}$$

describes the many-body dynamics of the system. Such a Hamiltonian is equivalent to a highly anisotropic Heisenberg model as the density interaction V_{ij} is two orders of magnitude larger than the hopping strength $|J_{ij}|$. The nonlocal density interaction V_{ij} also facilitates the study of many-body dynamics beyond the hard-core constraints. To verify the effective model and its distinct features, we first consider to implement a Harper-Hofstadter ladder. With dressing fields of four different colors introduced in Fig. 3(b), an arbitrary flux pattern can be realized [Fig. 3(c)]. For a symmetric pattern $\Phi_1 = \Phi_4$, $\Phi_2 = \Phi_3$, we calculate the trajectories for two colliding excitations initially localized at the corners. The exact simulation based on Eq. (1) shows significant repulsion between the excitations [Fig. 3(d)], in agreement with the calculation based on Eq. (5). We also note that the trajectories for two excitations are no longer symmetric when nonlocal interaction V_{ij} comes into play [61,62]. Such an interesting feature does not appear in systems with only hard-core constraints [Eq. (3)].

The ability to implement such effective models permits exploration of topological phenomena in the presence of strong and finite-range interactions. As an example [Fig. 4(a)], we consider two-excitation dynamics in an anisotropic Harper-Hofstadter lattice [63] where the nearest-neighbor hopping take on different strengths J_x and J_y along the x and y directions, respectively. The model can be realized with the similar scheme shown in Fig. 3(b). When the flux Φ is uniform and rational ($\Phi/2\pi = p/q$), the single-particle spectra split into q gapped topological bands linked by gapless edge modes. Remarkably, the finite-range density interaction can further lead to the emergence of chiral edge-mode bound states with large bond lengths as we will show below.

Let us consider first the case of two tightly bound excitations, separated by two lattice sites along the y direction as illustrated in Fig. 4(a). When the differences $D_1 = V_2 - V_1$, $D_2 = V_2 - V_4$, and $D_3 = V_2 - V_3$ between density interactions V_2 and V_1, V_3, V_4 [Fig. 4(a)] are much larger than the tunneling strength, we can perturbatively construct an effective Harper-Hofstadter lattice for the center-of-mass dynamics of the bound pair [Fig. 4(b)], which moves across the lattice with modified hopping strengths $J'_x = 2J^2_x/D_2$ and $J'_y = J^2_y/D_1 + J^2_y/D_3$. Most importantly, the effective magnetic flux $\Phi' = 2\Phi$ of the doublon increases to twice the single-particle flux. An interesting case emerges for $\Phi = 2\pi/3$ such that $\Phi' = 4\pi/3 \,(\text{mod}\, 2\pi) = -\Phi$. In this case we expect to observe the coexistence of single-excitation chiral edge state and topologically protected edge-mode bound state with opposite chirality.

When the above interaction difference is finite, the situation becomes complicated and an exact diagonalization is required [64,65]. Since the effective Hamiltonian is verified in Fig. 3(d), we will perform the calculation based on Eq. (5). For an infinitely extended lattice along the y direction with a finite number of sites along the x direction, the two-body eigenstate with a y-direction center-of-mass quasimomentum

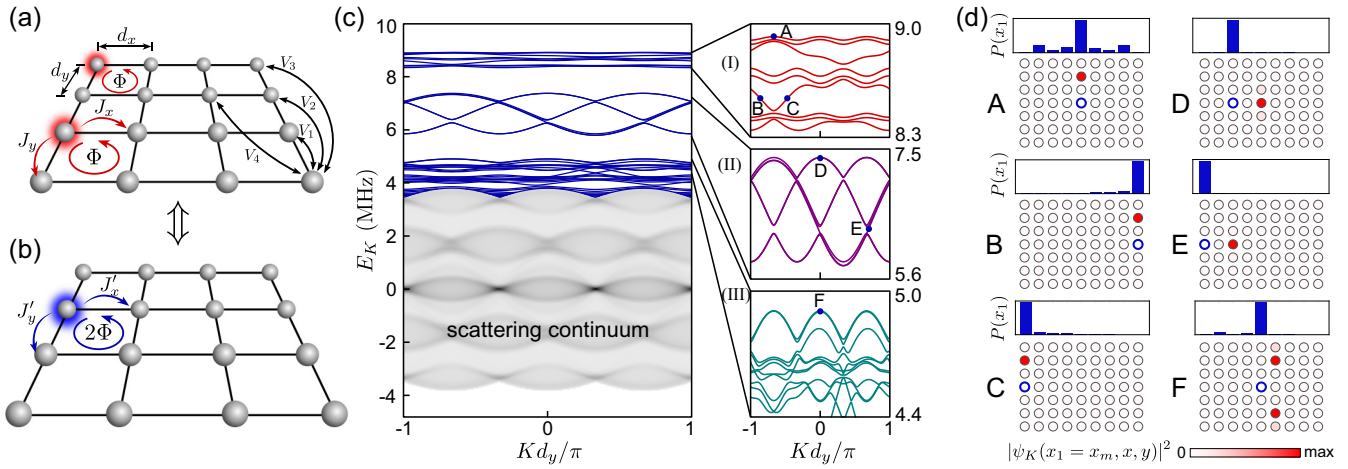

FIG. 4. (a) Anisotropic Harper-Hofstadter model with lattice constants d_x and d_y along x and y directions. A feasible implementation with $d_x = 5.1$, $d_y = 4.8$ μm, Rabi frequencies $\sim 2\pi \times 10$ MHz, and a ^{87}Rb-atom Rydberg state $|70S_{1/2}\rangle$ yields typical parameters $J_x = 0.5$ MHz, $J_x/J_y = 0.6$, and $(V_1, V_2, V_3, V_4)/J_x = (1045, 16, 1.4, 7.7)$. (b) Effective lattice for the center-of-mass motion of the bound pair shown in (a). (c) Two-body spectra of the system with nine sites along the x direction where different types (I)–(III) of bound pairs are distinguished by their orientations. (d) Density distribution for the first excitation $[P(x_1) = \sum_{x,y} |\psi_K(x_1, x, y)|^2]$ and the second excitation $(|\psi_K(x_1 = x_m, x, y)|^2$, scaled by shades of red) with $x_m = \arg_{\max}[P(x_1)]$ the most occupied site of the first excitation (blue empty circle).

K can be written as

$$|\psi_K\rangle = \frac{1}{2\pi} \sum_{\mathbf{r}_1 \neq \mathbf{r}_2} \psi_K(x_1, x_2, r) e^{iKR} \hat{b}^\dagger_{\mathbf{r}_1} \hat{b}^\dagger_{\mathbf{r}_2} |0\rangle, \tag{6}$$

where $r = y_2 - y_1$ and $R = (y_1 + y_2)/2$ denote the relative and center-of-mass coordinates along the y direction, $\hat{b}^\dagger_{\mathbf{r}_\nu}$ creates a Rydberg excitation at $\mathbf{r}_\nu = (x_\nu, y_\nu)$, and $|0\rangle$ is the vacuum state with all atoms in $|g\rangle$. The associated spectrum of eigenenergies E_K is shown in Fig. 4(c) and reveals a number of interesting states. The scattering continuum forms the lowest band with oscillating density of states. Above the scattering continuum, we identify different patterns of bound states. Figures 4(c) and 4(d) show the dispersion and density profile of three types of these states. The type-I bound state corresponds to the one depicted in Fig. 4(a), whose spectrum is split into three energy bands with Chern numbers $\mathcal{C} = \{-1, 2, -1\}$ (from the lowest to the highest) predicted by the center-of-mass motion analysis.

The state, marked as A in Fig. 4(c,I), is located in the upper band and represents a normal bound state in the bulk of the system. The other two states, marked as B and C, lie within the gap between the lowest and the middle bands and are topologically protected bound states that are respectively localized at the right and left edge of the lattice. Similar states can be identified for the type-II bound pair [Fig. 4(c,II)], which are aligned along the x direction, and form bulk-mode (marked as D) as well as chiral-edge-mode (marked as E) bound states. The finite range of the Rydberg-state interaction also makes it possible to form bound pairs separated by a longer distance, such as the type-III state, indicated in Fig. 4(c,III) and shown in panel F of Fig. 4(d).

Figure 5(a) shows the transport dynamics of a single-excitation edge mode and demonstrates counterclockwise propagation. The depicted motion around a finite lattice with edge defects indeed shows negligible backward scattering. The dynamics of the type-I bound state C [Figs. 4(c,I) and 4(d)] is displayed in Fig. 5(b). One clearly finds unidirectional doublon motion that is robust against local defects, and now features opposite chirality compared to the single-excitation transport. Figure 5(d) shows the two-body correlation function along the outer edge of the lattice [Fig. 5(c)] and demonstrates that the bound-state structure of the doublon indeed stays fully intact during its topologically protected transport.

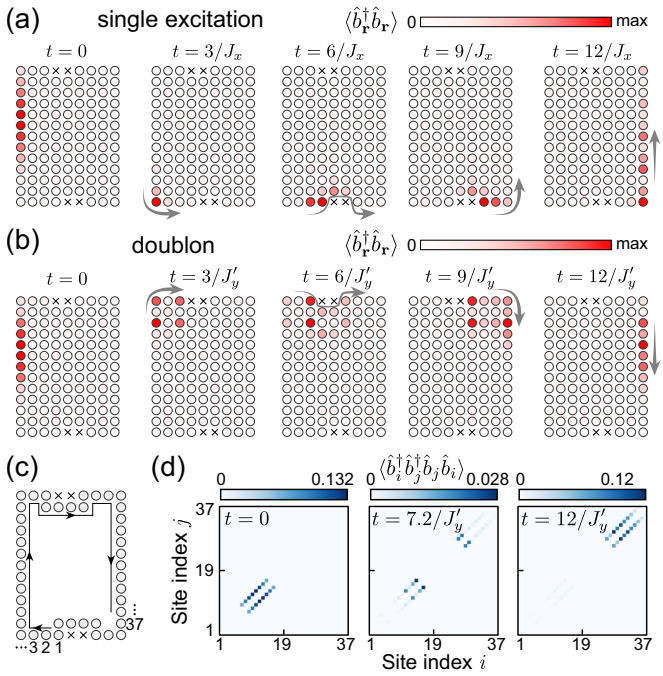

FIG. 5. (a) and (b) show evolution of the density distribution $\langle \hat{b}^\dagger_{\mathbf{r}} \hat{b}_{\mathbf{r}} \rangle$ for the lowest chiral edge mode of a single-excitation and a type-I bound pair, respectively. "×" denotes a vacancy defect. (c) Definition of the site index along the edge. (d) Evolution of the two-body correlation function $\langle \hat{b}^\dagger_i \hat{b}^\dagger_j \hat{b}_j \hat{b}_i \rangle$.

In conclusion, we have described the application of multicolor laser dressing to generate synthetic gauge fields for Rydberg excitations in neutral atom quantum simulators. Our approach makes it possible to realize arbitrary Peierls phases without compromising the accuracy of the quantum simulation. In particular, the scheme features individual tunability of the magnetic flux, which permits the experimental study of rich physics not yet explored with a nonuniform gauge field, e.g., exotic metal-insulator transition driven by the random flux [66–68], and emergence of anyons from a fractal flux pattern [69]. The inherent long-range interacting feature also motives future work on topological phenomena in interacting systems, such as emergent dynamical gauge fields [39,70] and fractional quantum Hall physics [71].

Note added. We recently became aware of two interesting schemes for realizing synthetic gauge fields in Rydberg-atom arrays, respectively, based on laser-assisted dipole-dipole interactions in a rectangular lattice [72] and Rydberg-dressing induced ground-state interactions in a honeycomb lattice [73].

We thank X. Li, X. Liang, C. Chen, A. E. B. Nielsen, A. L. Andersen, J. Yu, S. Guo, F. Chen, X.-C. Zhou, and R. Lin for valuable discussions. This work was supported by the National Key R&D Program of China (Grants No. 2018YFA0306504 and No. 2018YFA0306503), the National Natural Science Foundation of China (NSFC) (Grant No. 12174214), and by the Innovation Program for Quantum Science and Technology (Project No. 2-9-4). F.Y., K.M., and T.P. acknowledge the support from Carlsberg Foundation through the "Semper Ardens" Research Project QCooL and from the Danish National Research Foundation (DNRF) through the Center of Excellence "CCQ" (Grant No. DNRF156).

[1] I. M. Georgescu, S. Ashhab, and F. Nori, Quantum simulation, Rev. Mod. Phys. **86**, 153 (2014).
[2] H. L. Stormer, D. C. Tsui, and A. C. Gossard, The fractional quantum hall effect, Rev. Mod. Phys. **71**, S298 (1999).
[3] C. Nayak, S. H. Simon, A. Stern, M. Freedman, and S. Das Sarma, Non-abelian anyons and topological quantum computation, Rev. Mod. Phys. **80**, 1083 (2008).
[4] S. C. Zhang, T. H. Hansson, and S. Kivelson, Effective-Field-Theory Model for the Fractional Quantum Hall Effect, Phys. Rev. Lett. **62**, 82 (1989).
[5] X.-G. Wen, F. Wilczek, and A. Zee, Chiral spin states and superconductivity, Phys. Rev. B **39**, 11413 (1989).
[6] R. B. Laughlin and Z. Zou, Properties of the chiral-spin-liquid state, Phys. Rev. B **41**, 664 (1990).
[7] B. Bauer, L. Cincio, B. P. Keller, M. Dolfi, G. Vidal, S. Trebst, and A. W. Ludwig, Chiral spin liquid and emergent anyons in a kagome lattice mott insulator, Nat. Commun. **5**, 5137 (2014).
[8] S.-S. Gong, W. Zhu, and D. Sheng, Emergent chiral spin liquid: Fractional quantum hall effect in a kagome heisenberg model, Sci. Rep. **4**, 6317 (2014).
[9] E. J. Mueller, Artificial electromagnetism for neutral atoms: Escher staircase and laughlin liquids, Phys. Rev. A **70**, 041603(R) (2004).
[10] M. Aidelsburger, M. Atala, S. Nascimbene, S. Trotzky, Y.-A. Chen, and I. Bloch, Experimental Realization of Strong Effective Magnetic Fields in an Optical Lattice, Phys. Rev. Lett. **107**, 255301 (2011).
[11] H. Miyake, G. A. Siviloglou, C. J. Kennedy, W. C. Burton, and W. Ketterle, Realizing the Harper Hamiltonian with Laser-Assisted Tunneling in Optical Lattices, Phys. Rev. Lett. **111**, 185302 (2013).
[12] M. Aidelsburger, M. Atala, M. Lohse, J. T. Barreiro, B. Paredes, and I. Bloch, Realization of the Hofstadter Hamiltonian with Ultracold Atoms in Optical Lattices, Phys. Rev. Lett. **111**, 185301 (2013).
[13] B. Stuhl, H.-I. Lu, L. Aycock, D. Genkina, and I. Spielman, Visualizing edge states with an atomic bose gas in the quantum hall regime, Science **349**, 1514 (2015).
[14] J. Struck, C. Ölschläger, M. Weinberg, P. Hauke, J. Simonet, A. Eckardt, M. Lewenstein, K. Sengstock, and P. Windpassinger, Tunable Gauge Potential for Neutral and Spinless Particles in Driven Optical Lattices, Phys. Rev. Lett. **108**, 225304 (2012).
[15] A. R. Kolovsky, Creating artificial magnetic fields for cold atoms by photon-assisted tunneling, Europhys. Lett. **93**, 20003 (2011).
[16] G. Jotzu, M. Messer, R. Desbuquois, M. Lebrat, T. Uehlinger, D. Greif, and T. Esslinger, Experimental realization of the topological haldane model with ultracold fermions, Nature (London) **515**, 237 (2014).
[17] N. Goldman and J. Dalibard, Periodically Driven Quantum Systems: Effective Hamiltonians and Engineered Gauge Fields, Phys. Rev. X **4**, 031027 (2014).
[18] P. Roushan *et al.*, Chiral ground-state currents of interacting photons in a synthetic magnetic field, Nat. Phys. **13**, 146 (2017).
[19] T. Ozawa, H. M. Price, A. Amo, N. Goldman, M. Hafezi, L. Lu, M. C. Rechtsman, D. Schuster, J. Simon, O. Zilberberg *et al.*, Topological photonics, Rev. Mod. Phys. **91**, 015006 (2019).
[20] K. Fang, Z. Yu, and S. Fan, Photonic Aharonov-Bohm Effect Based on Dynamic Modulation, Phys. Rev. Lett. **108**, 153901 (2012).
[21] K. Fang, Z. Yu, and S. Fan, Realizing effective magnetic field for photons by controlling the phase of dynamic modulation, Nat. Photonics **6**, 782 (2012).
[22] F. Yang and Y. Li, Nonreciprocal diffraction of light based on double-transition-assisted photonic aharonov-bohm effect, Phys. Rev. B **94**, 165439 (2016).
[23] Y. Liu, X. Chen, and Y. Xu, Topological phononics: From fundamental models to real materials, Adv. Funct. Mater. **30**, 1904784 (2020).
[24] M. Schmidt, S. Kessler, V. Peano, O. Painter, and F. Marquardt, Optomechanical creation of magnetic fields for photons on a lattice, Optica **2**, 635 (2015).
[25] T. Manovitz, Y. Shapira, N. Akerman, A. Stern, and R. Ozeri, Quantum simulations with complex geometries and synthetic gauge fields in a trapped ion chain, PRX Quantum **1**, 020303 (2020).
[26] J. P. Mathew, J. Del Pino, and E. Verhagen, Synthetic gauge fields for phonon transport in a nano-optomechanical system, Nat. Nanotechnol. **15**, 198 (2020).

[27] P. Schauss, Quantum simulation of transverse ising models with rydberg atoms, Quantum Sci. Technol. **3**, 023001 (2018).

[28] X. Wu, X. Liang, Y. Tian, F. Yang, C. Chen, Y.-C. Liu, M. K. Tey, and L. You, A concise review of rydberg atom based quantum computation and quantum simulation, Chin. Phys. B **30**, 020305 (2021).

[29] M. Morgado and S. Whitlock, Quantum simulation and computing with rydberg-interacting qubits, AVS Quantum Sci. **3**, 023501 (2021).

[30] A. Browaeys and T. Lahaye, Many-body physics with individually controlled rydberg atoms, Nat. Phys. **16**, 132 (2020).

[31] P. Scholl, M. Schuler, H. J. Williams, A. A. Eberharter, D. Barredo, K.-N. Schymik, V. Lienhard, L.-P. Henry, T. C. Lang, T. Lahaye, A. M. Läuchli, and A. Browaeys, Quantum simulation of 2d antiferromagnets with hundreds of rydberg atoms, Nature (London) **595**, 233 (2021).

[32] D. Bluvstein, A. Omran, H. Levine, A. Keesling, G. Semeghini, S. Ebadi, T. T. Wang, A. A. Michailidis, N. Maskara, W. W. Ho, S. Choi, M. Serbyn, V. Vuletić, and M. Lukin, Controlling quantum many-body dynamics in driven rydberg atom arrays, Science **371**, 1355 (2021).

[33] S. Ebadi, T. T. Wang, H. Levine, A. Keesling, G. Semeghini, A. Omran, D. Bluvstein, R. Samajdar, H. Pichler, W. W. Ho, S. Choi, S. Sachdev, M. Greiner, V. Vuletić, and M. D. Lukin, Quantum phases of matter on a 256-atom programmable quantum simulator, Nature (London) **595**, 227 (2021).

[34] V. Bharti, S. Sugawa, M. Mizoguchi, M. Kunimi, Y. Zhang, S. de Léséleuc, T. Tomita, T. Franz, M. Weidemüller, and K. Ohmori, Ultrafast many-body dynamics in an ultracold rydberg-excited atomic mott insulator, arXiv:2201.09590.

[35] D. Peter, N. Y. Yao, N. Lang, S. D. Huber, M. D. Lukin, and H. P. Büchler, Topological bands with a chern number c = 2 by dipolar exchange interactions, Phys. Rev. A **91**, 053617 (2015).

[36] V. Lienhard, P. Scholl, S. Weber, D. Barredo, S. de Léséleuc, R. Bai, N. Lang, M. Fleischhauer, H. P. Büchler, T. Lahaye, and A. Browaeys, Realization of a Density-Dependent Peierls Phase in a Synthetic, Spin-Orbit Coupled Rydberg System, Phys. Rev. X **10**, 021031 (2020).

[37] S. Weber, S. De Léséleuc, V. Lienhard, D. Barredo, T. Lahaye, A. Browaeys, and H. P. Büchler, Topologically protected edge states in small rydberg systems, Quantum Sci. Technol. **3**, 044001 (2018).

[38] S. Weber, P. Bienias, and H. P. Büchler, Topological bands in the continuum using rydberg states, arXiv:2101.08363.

[39] S. Ohler, M. Kiefer-Emmanouilidis, A. Browaeys, H. P. Büchler, and M. Fleischhauer, Self-generated quantum gauge fields in arrays of rydberg atoms, New J. Phys. **24**, 023017 (2022).

[40] S. Weber, R. Bai, N. Makki, J. Mögerle, T. Lahaye, A. Browaeys, M. Daghofer, N. Lang, and H. P. Büchler, Experimentally accessible scheme for a fractional chern insulator in rydberg atoms, PRX Quantum **3**, 030302 (2022).

[41] S. Ohler, M. Kiefer-Emmanouilidis, and M. Fleischhauer, Quantum spin liquids of rydberg excitations in a honeycomb lattice induced by density-dependent peierls phases, arXiv:2202.03860.

[42] G. Salerno, M. Di Liberto, C. Menotti, and I. Carusotto, Topological two-body bound states in the interacting haldane model, Phys. Rev. A **97**, 013637 (2018).

[43] G. Salerno, G. Palumbo, N. Goldman, and M. Di Liberto, Interaction-induced lattices for bound states: Designing flat bands, quantized pumps, and higher-order topological insulators for doublons, Phys. Rev. Res. **2**, 013348 (2020).

[44] A. Berti and I. Carusotto, Topological two-particle dynamics in a periodically driven lattice model with on-site interactions, Phys. Rev. A **105**, 023329 (2022).

[45] M. Aidelsburger, M. Lohse, C. Schweizer, M. Atala, J. T. Barreiro, S. Nascimbène, N. Cooper, I. Bloch, and N. Goldman, Measuring the chern number of hofstadter bands with ultracold bosonic atoms, Nat. Phys. **11**, 162 (2015).

[46] J. Zeiher, R. Van Bijnen, P. Schauß, S. Hild, J.-y. Choi, T. Pohl, I. Bloch, and C. Gross, Many-body interferometry of a rydberg-dressed spin lattice, Nat. Phys. **12**, 1095 (2016).

[47] F. Yang, S. Yang, and L. You, Quantum Transport of Rydberg Excitons with Synthetic Spin-Exchange Interactions, Phys. Rev. Lett. **123**, 063001 (2019).

[48] F. Yang, Y.-C. Liu, and Li. You, Atom-Photon Spin-Exchange Collisions Mediated by Rydberg Dressing, Phys. Rev. Lett. **125**, 143601 (2020).

[49] See Supplemental Material at http://link.aps.org/supplemental/10.1103/PhysRevResearch.4.L032046 for details on derivations of the effective Hamiltonians, tunability of our model, robustness against decoherence, and a feasible experimental implementation, which includes Ref. [74–82].

[50] The vdW coefficient is taken to be $C_6 = 2\pi \times 1029\ \mathrm{GHz}\,\mu\mathrm{m}^6$ (for the $|70S_{1/2}\rangle$ state of the ^{87}Rb atom), and the lattice constant is 3 μm in (a) and 6 μm in (d). The Rabi frequencies are chosen according to $\Omega_{\Theta'} = \Omega_a\sqrt{\Delta_{\Theta'}(\Delta_{\Theta'}+V)/\Delta_A(\Delta_A+V)}$ with $\Theta' = B, C, D$ such that the nearest-neighbor hopping take the same strength. In order to balance the on-site potential μ_i, the detuning of each field is slightly shifted at each site [49]. The center-of-mass trajectories for the left and right regions in (c) are defined as $\bar{\mathbf{r}}_L = \sum_{x\leqslant 0}\mathbf{r}P_\mathbf{r}/\sum_{x\leqslant 0}P_\mathbf{r}$ and $\bar{\mathbf{r}}_R = \sum_{x\geqslant 0}\mathbf{r}P_\mathbf{r}/\sum_{x\geqslant 0}P_\mathbf{r}$ with $\mathbf{r} = (x, y)$, and $P_\mathbf{r}$ is the time-dependent occupation probability at the site $\mathbf{r}$.

[51] M. Bukov, L. D'Alessio, and A. Polkovnikov, Universal high-frequency behavior of periodically driven systems: From dynamical stabilization to floquet engineering, Adv. Phys. **64**, 139 (2015).

[52] A. Eckardt and E. Anisimovas, High-frequency approximation for periodically driven quantum systems from a floquet-space perspective, New J. Phys. **17**, 093039 (2015).

[53] M. S. Rudner and N. H. Lindner, The floquet engineer's handbook, arXiv:2003.08252.

[54] X. Li, J. You, X. Shao, and W. Li, Coherent ground-state transport of neutral atoms, Phys. Rev. A **105**, 032417 (2022).

[55] S.-K. Son, S. Han, and S.-I. Chu, Floquet formulation for the investigation of multiphoton quantum interference in a superconducting qubit driven by a strong ac field, Phys. Rev. A **79**, 032301 (2009).

[56] T.-S. Ho and S.-I. Chu, Semiclassical many-mode floquet theory. iv. coherent population trapping and su (3) dynamical evolution of dissipative three-level systems in intense bichromatic fields, Phys. Rev. A **32**, 377 (1985).

[57] P. Aravind and J. Hirschfelder, Two-state systems in semiclassical and quantized fields, J. Phys. Chem. **88**, 4788 (1984).

[58] I. Shavitt and L. T. Redmon, Quasidegenerate perturbation theories. a canonical van vleck formalism and its relationship to other approaches, J. Chem. Phys. **73**, 5711 (1980).

[59] D. A. Lidar, I. L. Chuang, and K. B. Whaley, Decoherence-Free Subspaces for Quantum Computation, Phys. Rev. Lett. **81**, 2594 (1998).

[60] L.-N. Sun, F.-Q. Guo, Z. Shan, M. Feng, L.-L. Yan, and S.-L. Su, One-step implementation of Rydberg nonadiabatic noncyclic geometric quantum computation in decoherence-free subspaces, Phys. Rev. A **105**, 062602 (2022).

[61] J. Yu, N. Sun, and H. Zhai, Symmetry Protected Dynamical Symmetry in the Generalized Hubbard Models, Phys. Rev. Lett. **119**, 225302 (2017).

[62] M. E. Tai, A. Lukin, M. Rispoli, R. Schittko, T. Menke, D. Borgnia, P. M. Preiss, F. Grusdt, A. M. Kaufman, and M. Greiner, Microscopy of the interacting harper–hofstadter model in the two-body limit, Nature (London) **546**, 519 (2017).

[63] Q.-Y. Liang, D. Trypogeorgos, A. Valdés-Curiel, J. Tao, M. Zhao, and I. B. Spielman, Coherence and decoherence in the harper-hofstadter model, Phys. Rev. Res. **3**, 023058 (2021).

[64] F. Letscher and D. Petrosyan, Mobile bound states of rydberg excitations in a lattice, Phys. Rev. A **97**, 043415 (2018).

[65] T. Macrì, L. Lepori, G. Pagano, M. Lewenstein, and L. Barbiero, Bound state dynamics in the long-range spin-1/2 XXZ model, Phys. Rev. B **104**, 214309 (2021).

[66] S.-C. Zhang and D. P. Arovas, Effective field theory of electron motion in the presence of random magnetic flux, Phys. Rev. Lett. **72**, 1886 (1994).

[67] A. Furusaki, Anderson Localization due to a Random Magnetic Field in Two Dimensions, Phys. Rev. Lett. **82**, 604 (1999).

[68] C.-A. Li, S.-B. Zhang, J. C. Budich, and B. Trauzettel, Transition from metal to higher-order topological insulator driven by random flux, Phys. Rev. B **106**, L081410 (2022).

[69] S. Manna, C. W. Duncan, C. A. Weidner, J. F. Sherson, and A. E. B. Nielsen, Anyon braiding on a fractal lattice with a local hamiltonian, Phys. Rev. A **105**, L021302 (2022).

[70] L. Homeier, A. Bohrdt, S. Linsel, E. Demler, J. C. Halimeh, and F. Grusdt, Quantum simulation of $\mathbb{Z}_2$ lattice gauge theories with dynamical matter from two-body interactions in (2+1)D, arXiv:2205.08541.

[71] N. Y. Yao, C. R. Laumann, A. V. Gorshkov, S. D. Bennett, E. Demler, P. Zoller, and M. D. Lukin, Topological Flat Bands from Dipolar Spin Systems, Phys. Rev. Lett. **109**, 266804 (2012).

[72] T.-H. Yang, B.-Z. Wang, X.-C. Zhou, and X.-J. Liu, Quantum hall states for rydberg atoms with laser-assisted dipole-dipole interactions, Phys. Rev. A **106**, L021101 (2022).

[73] Y. Zhao and X.-F. Shi, The fractional chern insulator with rydberg-dressed neutral atoms, arXiv:2206.04213.

[74] A. Omran, H. Levine, A. Keesling, G. Semeghini, T. T. Wang, S. Ebadi, H. Bernien, A. S. Zibrov, H. Pichler, S. Choi, J. Cui, M. Rossignolo, P. Rembold, S. Montangero, T. Calarco, M. Endres, M. Greiner, V. Vuletić, and M. D. Lukin, Generation and manipulation of schrödinger cat states in rydberg atom arrays, Science **365**, 570 (2019).

[75] S. de Léséleuc, D. Barredo, V. Lienhard, A. Browaeys, and T. Lahaye, Analysis of imperfections in the coherent optical excitation of single atoms to rydberg states, Phys. Rev. A **97**, 053803 (2018).

[76] H. Levine, A. Keesling, A. Omran, H. Bernien, S. Schwartz, A. S. Zibrov, M. Endres, M. Greiner, V. Vuletić, and M. D. Lukin, High-Fidelity Control and Entanglement of Rydberg-Atom Qubits, Phys. Rev. Lett. **121**, 123603 (2018).

[77] J. M. Moix, M. Khasin, and J. Cao, Coherent quantum transport in disordered systems: I. the influence of dephasing on the transport properties and absorption spectra on one-dimensional systems, New J. Phys. **15**, 085010 (2013).

[78] A. Cooper, J. P. Covey, I. S. Madjarov, S. G. Porsev, M. S. Safronova, and M. Endres, Alkaline-Earth Atoms in Optical Tweezers, Phys. Rev. X **8**, 041055 (2018).

[79] N. Lorenz, L. Festa, L.-M. Steinert, and C. Gross, Raman sideband cooling in optical tweezer arrays for rydberg dressing, SciPost Phys. **10**, 052 (2021).

[80] I. I. Beterov, I. I. Ryabtsev, D. B. Tretyakov, and V. M. Entin, Quasiclassical calculations of blackbody-radiation-induced depopulation rates and effective lifetimes of rydberg n s, n p, and n d alkali-metal atoms with n 80, Phys. Rev. A **79**, 052504 (2009).

[81] L. Wu, S. Cheng, and S. Tao, Simultaneous shaping of amplitude and phase of light in the entire output plane with a phase-only hologram, Sci. Rep. **5**, 15426 (2015).

[82] D. Bowman, T. L. Harte, V. Chardonnet, C. De Groot, S. J. Denny, G. Le Goc, M. Anderson, P. Ireland, D. Cassettari, and G. D. Bruce, High-fidelity phase and amplitude control of phase-only computer generated holograms using conjugate gradient minimisation, Opt. Express **25**, 11692 (2017).